12

Resistance of a Molecule

Magnus Paulsson
Purdue University

Ferdows Zahid
Purdue University

Supriyo Datta
Purdue University

CONTENTS

12.1 Introduction

In recent years, several experimental groups have reported measurements of the current–voltage (I-V) characteristics of individual or small numbers of molecules. Even three-terminal measurements showing evidence of transistor action have been reported using carbon nanotubes[1,2] as well as self-assembled monolayers of conjugated polymers.[3] These developments have attracted much attention from the semiconductor industry, and there is great interest from an applied point of view to model and understand the capabilities of molecular conductors. At the same time, this is also a topic of great interest from the point of view of basic physics. A molecule represents a quantum dot, at least an order of magnitude smaller than semiconductor quantum dots, which allows us to study many of the same mesoscopic and/or many-body effects at far higher temperatures.

So what is the resistance of a molecule? More specifically, what do we see when we connect a short molecule between two metallic contacts as shown in Figure 12.1 and measure the current (I) as a function of the voltage (V)? Most commonly we get I-V characteristics of the type sketched in Figure 12.2. This has been observed using many different approaches including breakjunctions,[4–8] scanning probes,[9–12] nanopores,[13] and a host of other methods (see, for example, Reference 14). A number of theoretical models have been developed for calculating the I-V characteristics of molecular wires using semi-empirical[12,15–18] as well as first-principles[19–25] theory.

Our purpose in this chapter is to provide an intuitive explanation for the observed I-V characteristics using simple models to illustrate the basic physics. However, it should be noted that molecular electronics is a rapidly developing field, and much of the excitement arises from the possibility of discovering novel physics beyond the paradigms discussed here. To cite a simple example, very few experiments to date[3] incorporate the gate electrode shown in Figure 12.1, and we will largely ignore the gate in this chapter.

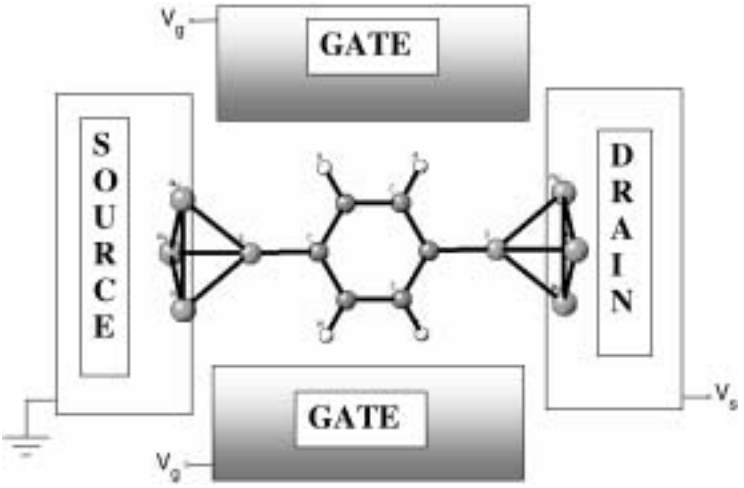

FIGURE 12.1 Conceptual picture of a "molecular transistor" showing a short molecule (Phenyl dithiol, PDT) sandwiched between source and drain contacts. Most experiments so far lack good contacts and do not incorporate the gate electrodes.

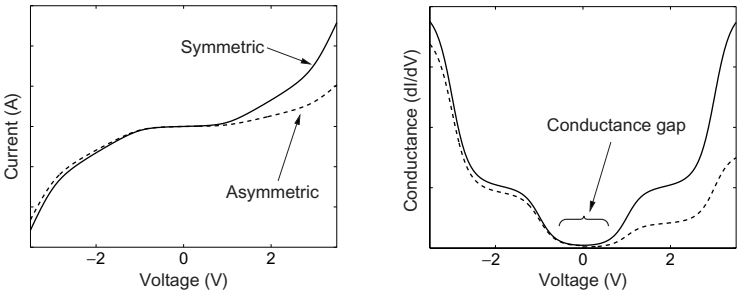

FIGURE 12.2 Schematic picture, showing general properties of measured current–voltage (I-V) and conductance (G-V) characteristics for molecular wires. Solid line, symmetrical I-V. Dashed line, asymmetrical I-V.

However, the gate electrode can play a significant role in shaping the I-V characteristics and deserves more attention. This is easily appreciated by looking at the applied potential profile U_{app} generated by the electrodes in the absence of the molecule. This potential profile satisfies the Laplace equation without any net charge anywhere and is obtained by solving:

$$\nabla \cdot (\varepsilon \nabla U_{\text{app}}) = 0 \tag{12.1}$$

subject to the appropriate boundary values on the electrodes (Figure 12.3). It is apparent that the electrode geometry has a significant influence on the potential profile that it imposes on the molecular species, and this could obviously affect the I-V characteristics in a significant way. After all, it is well known that a three-terminal metal/oxide/semiconductor field-effect transistor (MOSFET) with a gate electrode has a very different I-V characteristic compared with a two terminal n-i-n diode. The current in a MOSFET saturates under increasing bias, but the current in an n-i-n diode keeps increasing indefinitely. In contrast to the MOSFET, whose I-V is largely dominated by classical electrostatics, the I-V characteristics of molecules is determined by a more interesting interplay between nineteenth-century physics (electrostatics) and twentieth-century physics (quantum transport); and it is important to do justice to both aspects.

We will start in Section 12.2 with a qualitative discussion of the main factors affecting the I-V characteristics of molecular conductors, using a simple toy model to illustrate their role. However, this toy model misses two important factors: (1) shift in the energy level due to *charging effects* as the molecule

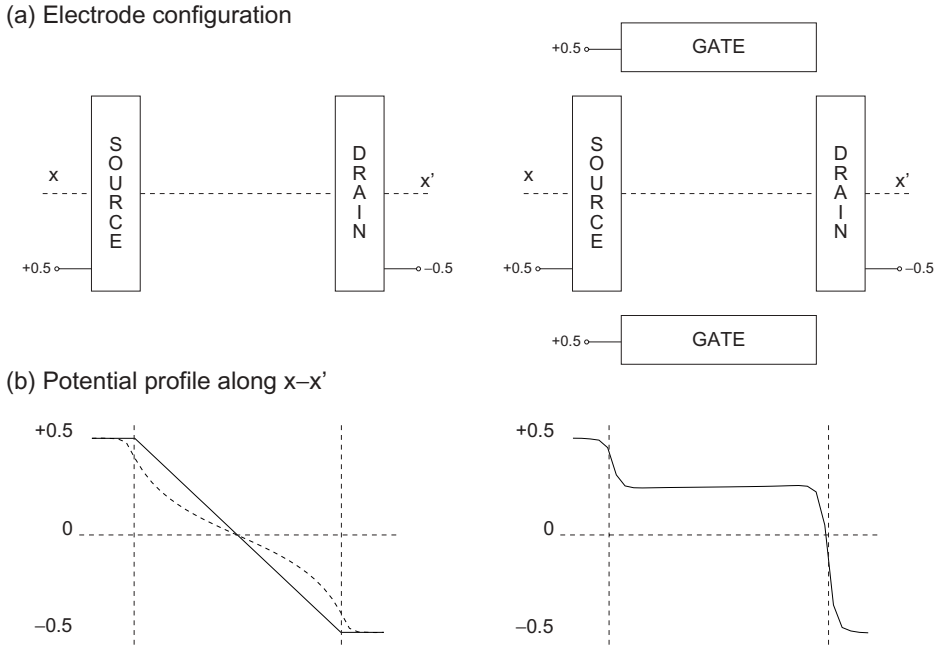

FIGURE 12.3 Schematic picture, showing potential profile for two geometries, without gate (left) and with gate (right).

loses or gains electrons and (2) *broadening* of the energy levels due to their finite lifetime arising from the coupling (Γ_1 and Γ_2) to the two contacts. Once we incorporate these effects (Section 12.3) we obtain more realistic I-V plots, even though the toy model assumes that conduction takes place independently through individual molecular levels. In general, however, multiple energy levels are simultaneously involved in the conduction process. In Section 12.4 we will describe the nonequilibrium Green's function (NEGF) formalism, which can be viewed as a generalized version of the one-level model to include multiple levels or conduction channels. This formalism provides a convenient framework for describing quantum transport[26] and can be used in conjunction with *ab initio* or semi-empirical Hamiltonians as described in a set of related articles.[27,28] Then in Section 12.5 we will illustrate the NEGF formalism with a simple semi-empirical model for a gold wire, n atoms long and one atom in cross-section. We could call this a Au_n molecule, though that is not how one normally thinks of a gold wire. However, this example is particularly instructive because it shows the lowest possible *resistance of a molecule* per channel, which is $\pi\hbar/e^2 = 12.9\ k\Omega$.[29]

12.2 Qualitative Discussion

12.2.1 Where Is the Fermi Energy?

Energy-Level Diagram: The first step in understanding the current (I) vs. voltage (V) curve for a molecular conductor is to draw an energy-level diagram and locate the Fermi energy. Consider first a molecule sandwiched between two metallic contacts but with very weak electronic coupling. We could then line up the energy levels as shown in Figure 12.4 using the metallic work function (WF), the electronic affinity (EA), and ionization potential (IP) of the molecule. For example, a (111) gold surface has a work function of ~ 5.3 eV, while the electron affinity and ionization potential, EA_0 and IP_0, for isolated phenyl dithiol (Figure 12.1) in the gas phase have been reported to be ~ 2.4 eV and 8.3 eV, respectively.[30] These values are associated with electron emission and injection to and from a vacuum and may need some modification to account for the metallic contacts. For example, the actual EA, IP will possibly be modified from EA_0, IP_0 due to the image potential W_{im} associated with the metallic contacts:[31]

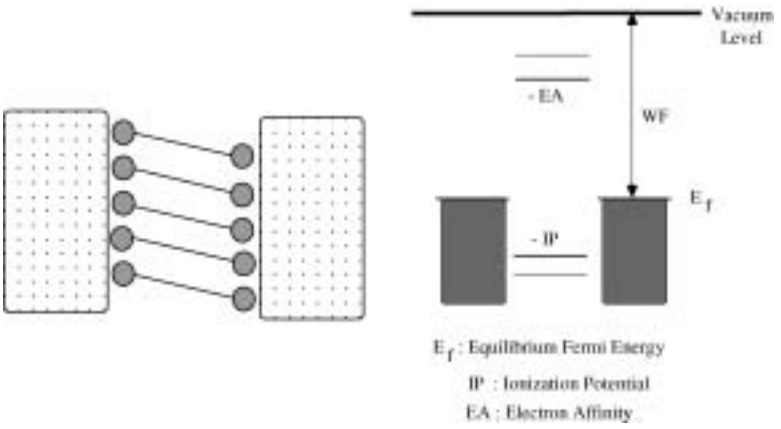

FIGURE 12.4 Equilibrium energy level diagram for a metal–molecule–metal sandwich for a weakly coupled molecule.

$$EA = EA_0 + W_{im} \tag{12.2}$$

$$IP = IP_0 - W_{im} \tag{12.3}$$

The probability of the molecule losing an electron to form a positive ion is equal to $e^{(WF\text{-}1P)/k_BT}$, while the probability of the molecule gaining an electron to form a negative ion is equal to $e^{(EA\text{-}WF)/k_BT}$. We thus expect the molecule to remain neutral as long as both $(IP - WF)$ and $(WF - EA)$ are much larger than k_BT, a condition that is usually satisfied for most metal–molecule combinations. Because it costs too much energy to transfer one electron into or out of the molecule, it prefers to remain neutral in equilibrium.

The picture changes qualitatively if the molecule is chemisorbed directly on the metallic contact (Figure 12.5). The molecular energy levels are now broadened significantly by the strong hybridization with the delocalized metallic wave functions, making it possible to transfer fractional amounts of charge to or from the molecule. Indeed there is a charge transfer, which causes a change in the electrostatic potential inside the molecule; and the energy levels of the molecule are shifted by a contact potential (CP), as shown.

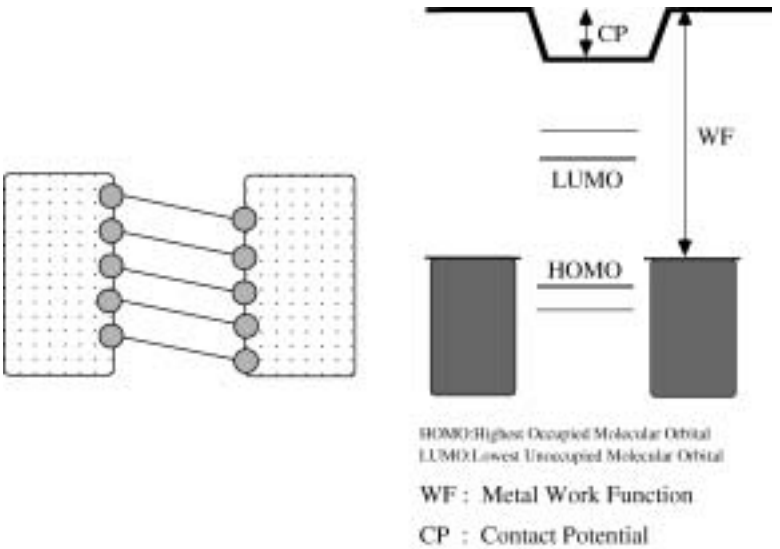

FIGURE 12.5 Equilibrium energy level diagram for a metal–molecule–metal sandwich for a molecule strongly coupled to the contacts.

It is now more appropriate to describe transport in terms of the HOMO–LUMO levels associated with incremental charge transfer[32] rather than the affinity and ionization levels associated with integer charge transfer. Whether the molecule–metal coupling is strong enough for this to occur depends on the relative magnitudes of the single electron charging energy (U) and energy level broadening (Γ). As a rule of thumb, if $U >> \Gamma$, we can expect the structure to be in the Coulomb Blockade (CB) regime characterized by integer charge transfer; otherwise it is in the self-consistent field (SCF) regime characterized by fractional charge transfer. This is basically the same criterion that one uses for the Mott transition in periodic structures, with Γ playing the role of the hopping matrix element. It is important to note that, for a structure to be in the CB regime, both contacts must be weakly coupled, as the total broadening Γ is the sum of the individual broadening due to the two contacts. Even if only one of the contacts is coupled strongly, we can expect $\Gamma \sim U$, thus putting the structure in the SCF regime. Figure 12.14 in Section 12.3.2 illustrates the I-V characteristics in the CB regime using a toy model. However, a moderate amount of broadening destroys this effect (see Figure 12.17), and in this chapter we will generally assume that the conduction is in the SCF regime.

Location of the Fermi energy: The location of the Fermi energy relative to the HOMO and LUMO levels is probably the most important factor in determining the current (I) vs. voltage (V) characteristics of molecular conductors. Usually it lies somewhere inside the HOMO–LUMO gap. To see this, we first note that E_f is located by the requirement that the number of states below the Fermi energy must be equal to the number of electrons in the molecule. But this number need not be equal to the integer number we expect for a neutral molecule. A molecule does not remain exactly neutral when connected to the contacts. It can and does pick up a fractional charge depending on the work function of the metal. However, the charge transferred (δn) for most metal–molecule combinations is usually much less than one. If δn were equal to +1, the Fermi energy would lie on the LUMO; while if δn were –1, it would lie on the HOMO. Clearly for values in between, it should lie somewhere in the HOMO–LUMO gap.

A number of authors have performed detailed calculations to locate the Fermi energy with respect to the molecular levels for a phenyl dithiol molecule sandwiched between gold contacts, but there is considerable disagreement. Different theoretical groups have placed it close to the LUMO[16,21] or to the HOMO.[12,19] The density of states inside the HOMO–LUMO gap is quite small, making the precise location of the Fermi energy very sensitive to small amounts of electron transfer — a fact that could have a significant effect on both theory and experiment. As such it seems justifiable to treat E_f as a fitting parameter within reasonable limits when trying to explain experimental I-V curves.

Broadening by the contacts: Common sense suggests that the strength of coupling of the molecule to the contacts is important in determining the current flow — the stronger the coupling, the larger the current. A useful quantitative measure of the coupling is the resulting broadening Γ of the molecular energy levels, see Figure 12.6. This broadening Γ can also be related to the time τ it takes for an electron placed in that level to escape into the contact: $\Gamma = \hbar/\tau$. In general, the broadening Γ could be different for different energy levels. Also it is convenient to define two quantities Γ_1 and Γ_2, one for each contact, with the total broadening $\Gamma = \Gamma_1 + \Gamma_2$.

One subtle point: Suppose an energy level is located well below the Fermi energy in the contact, so that the electrons are prevented from escaping by the exclusion principle. Would Γ be zero? No, the broadening would still be Γ, independent of the degree of filling of the contact as discussed in Reference 26. This observation is implicit in the NEGF formalism, though we do not invoke it explicitly.

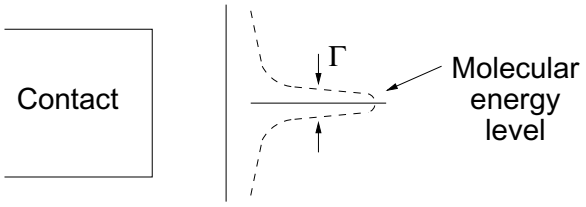

FIGURE 12.6 Energy level broadening.

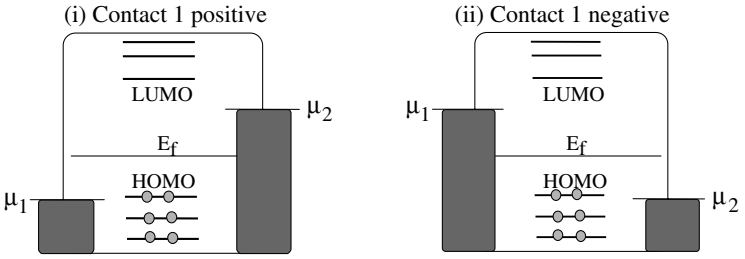

FIGURE 12.7 Schematic energy level diagram of metal–molecule–metal structure when contact 1 is (i) positively biased and when contact 1 is (ii) negatively biased with respect to contact 2.

12.2.2 Current Flow as a Balancing Act

Once we have drawn an equilibrium energy-level diagram, we can understand the process of current flow, which involves a nonequilibrium situation where the different reservoirs (e.g., the source and the drain) have different electrochemical potentials μ (Figure 12.7). For example, if a positive voltage V is applied externally to the drain with respect to the source, then the drain has an electrochemical potential lower than that of the source by eV : $\mu_2 = \mu_1 - eV$. The source and drain contacts thus have different Fermi functions, and each seeks to bring the active device into equilibrium with itself. The source keeps pumping electrons into it, hoping to establish equilibrium. But equilibrium is never achieved as the drain keeps pulling electrons out in its bid to establish equilibrium with itself. The device is thus forced into a balancing act between two reservoirs with different agendas that send it into a nonequilibrium state intermediate between what the source and drain would like to see. To describe this balancing process we need a kinetic equation that keeps track of the in- and out-flow of electrons from each of the reservoirs.

Kinetic equation: This balancing act is easy to see if we consider a simple one-level system, biased such that the energy ε lies in between the electrochemical potentials of the two contacts (Figure 12.8). An electron in this level can escape into contacts 1 and 2 at a rate of $\Gamma_1/\hbar$ and $\Gamma_2/\hbar$, respectively. If the level were in equilibrium with contact 1, then the number of electrons occupying the level would be given by

$$N_1 = 2(\text{for spin})\, f(\varepsilon, \mu_1) \tag{12.4}$$

where

$$f(\varepsilon, \mu) = \frac{1}{1 + e^{\frac{\varepsilon - \mu}{k_B T}}} \tag{12.5}$$

is the Fermi function. Similarly, if the level were in equilibrium with contact 2, the number would be:

$$N_2 = 2(\text{for spin})\, f(\varepsilon, \mu_2) \tag{12.6}$$

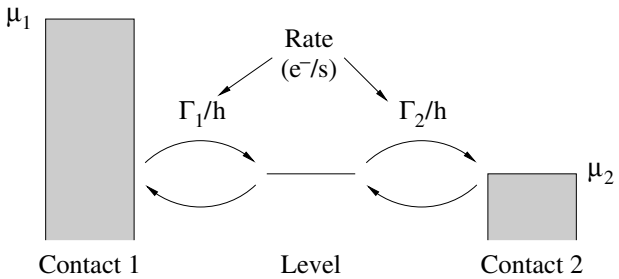

FIGURE 12.8 Illustration of the kinetic equation.

Under nonequilibrium conditions, the number of electrons N will be somewhere in between N_1 and N_2. To determine this number we write a steady-state *kinetic equation* that equates the net current at the left junction:

$$I_L = \frac{e\Gamma_1}{\hbar}(N_1 - N) \tag{12.7}$$

to the net current at the right junction:

$$I_R = \frac{e\Gamma_2}{\hbar}(N - N_2) \tag{12.8}$$

Steady state requires $I_L = I_R$, from which we obtain

$$N = 2\frac{\Gamma_1 f(\varepsilon, \mu_1) + \Gamma_2 f(\varepsilon, \mu_2)}{\Gamma_1 + \Gamma_2} \tag{12.9}$$

so that from Equation (12.7) or Equation (12.8) we obtain the current:

$$I = \frac{2e}{\hbar}\frac{\Gamma_1\Gamma_2}{\Gamma_1 + \Gamma_2}(f(\varepsilon, \mu_1) - f(\varepsilon, \mu_2)) \tag{12.10}$$

Equation (12.10) follows very simply from an elementary model, but it serves to illustrate a basic fact about the process of current flow. No current will flow if $f(\varepsilon, \mu_1) = f(\varepsilon, \mu_2)$. A level that is way below both electrochemical potentials μ_1 and μ_2 will have $f(\varepsilon, \mu_1) = f(\varepsilon, \mu_2) = 1$ and will not contribute to the current, just like a level that is way above both potentials μ_1 and μ_2 and has $f(\varepsilon, \mu_1) = f(\varepsilon, \mu_2) = 0$. It is only when the level lies between μ_1 and μ_2 (or within a few k_BT of μ_1 and μ_2) that we have $f(\varepsilon, \mu_1) \neq f(\varepsilon, \mu_2)$, and a current flows. Current flow is thus the result of the *difference in opinion* between the contacts. One contact would like to see more electrons (than N) occupy the level and keeps pumping them in, while the other would like to see fewer than N electrons and keeps pulling them out. The net effect is a continuous transfer of electrons from one contact to another.

Figure 12.9 shows a typical I vs. V calculated from Equation (12.10), using the parameters indicated in the caption. At first the current is zero because both μ_1 and μ_2 are above the energy level.

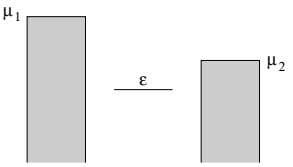

Once μ_2 drops below the energy level, the current increases to I_{max}, which is the maximum current that can flow through one level and is obtained from Equation (12.10) by setting $f(\varepsilon, \mu_1) = 1$ and $f(\varepsilon, \mu_2) = 0$:

$$I_{max} = \frac{2e}{\hbar}\Gamma_{\text{eff}} = \frac{2e}{\hbar}\frac{\Gamma_1\Gamma_2}{\Gamma_1 + \Gamma_2} \tag{12.11}$$

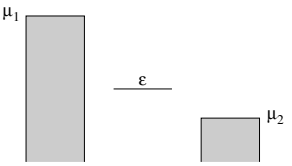

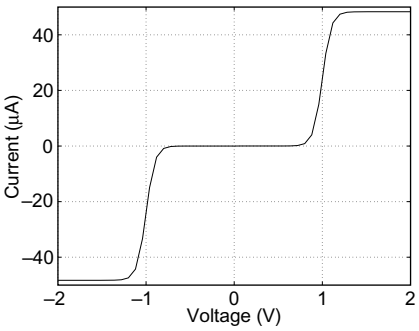

FIGURE 12.9 The current–voltage (I-V) characteristics for our toy model with $\mu_1 = E_f - eV/2$, $\mu_2 = E_f + eV/2$, $E_f = -5.0$ eV, $\varepsilon_0 = -5.5$ eV and $\Gamma_1 = \Gamma_2 = 0.2$ eV. MATLAB code in Section 12.A.1 ($U = 0$).

Note that in Figure 12.9 we have set $\mu_1 = E_f - eV/2$ and $\mu_2 = E_f + eV/2$. We could, of course, just as well have set $\mu_1 = E_f - eV$ and $\mu_1 = E_f$. But the average potential in the molecule would be $-V/2$ and we would need to shift ε appropriately. It is more convenient to choose our reference such that the average molecular potential is zero, and there is no need to shift ε.

Note that the current is proportional to Γ_{eff}, which is the parallel combination of Γ_1 and Γ_2. This seems quite reasonable if we recognize that Γ_1 and Γ_2 represent the strength of the coupling to the two contacts and as such are like two *conductances in series*. For long conductors we would expect a third conductance in series representing the actual conductor. This is what we usually have in mind when we speak of conductance. But short conductors have virtually zero resistance, and what we measure is essentially the contact or interface resistance.* This is an important conceptual issue that caused much argument and controversy in the 1980s. It was finally resolved when experimentalists measured the conductance of very short conductors and found it approximately equal to $2e^2/h$, which is a fundamental constant equal to 77.8 μA/V. The inverse of this conductance $h/2e^2 = 12.9$ kΩ is now believed to represent the minimum contact resistance that can be achieved for a one-channel conductor. Even a copper wire with a one-atom cross-section will have a resistance at least this large. Our simple one-level model (Figure 12.9) does not predict this result because we have treated the level as discrete, but the more complete treatment in later sections will show it.

12.3 Coulomb Blockade?

As we mentioned in Section 12.2, a basic question we need to answer is whether the process of conduction through the molecule belongs to the Coulomb Blockade (CB) or the Self-Consistent Field (SCF) regime. In this section, we will first discuss a simple model for charging effects (Section 12.3.1) and then look at the distinction between the simple SCF regime and the CB regime (Section 12.3.2). Finally, in Section 12.3.3 we show how moderate amounts of level broadening often destroy CB effects, making a simple SCF treatment quite accurate.

12.3.1 Charging Effects

Given the level (ε), broadening (Γ_1, Γ_2), and the electrochemical potentials μ_1 and μ_2 of the two contacts, we can solve Equation (12.10) for the current I. But we want to include charging effects in the calculations. Therefore, we add a potential U_{SCF} due to the change in the number of electrons from the equilibrium value ($f_0 = f(\varepsilon_0, E_f)$):

* Four-terminal measurements have been used to separate the contact from the device resistance (see, for example, Reference 33).

$$U_{SCF} = U(N - 2f_0) \tag{12.12}$$

similar to a Hubbard model. We then let the level ε float up or down by this potential:

$$\varepsilon = \varepsilon_0 + U_{SCF} \tag{12.13}$$

Because the potential depends on the number of electrons, we need to calculate the potential using the self-consistent procedure shown in Figure 12.10.

Once the converged solution is obtained, the current is calculated from Equation (12.10). This very simple model captures much of the observed physics of molecular conduction. For example, the results obtained by setting $E_f = -5.0$ eV, $\varepsilon_0 = -5.5$ eV, $\Gamma_1 = 0.2$ eV, $\Gamma_2 = 0.2$ eV are shown in Figure 12.11 with ($U = 1.0$ eV) and without ($U = 0$ eV) charging effects. The finite width of the conductance peak (with $U = 0$) is due to the temperature used in the calculations ($k_BT = 0.025$ eV). Note how the inclusion of charging tends to broaden the sharp peaks in conductance, even though we have not included any extra level broadening in this calculation. The size of the conductance gap is directly related to the energy difference between the molecular energy level and the Fermi energy. The current starts to increase when the voltage reaches 1 V, which is exactly $2|E_f - \varepsilon_0|$, as would be expected even from a theory with no charging. Charging enters the picture only at higher voltages, when a chemical potential tries to cross the level. The energy level shifts in energy (Equation (12.13)) if the charging energy is nonzero. Thus, for a small charging energy, the chemical potential easily crosses the level, giving a sharp increase of the current. If the charging energy is large, the current increases gradually because the energy level follows the chemical potential due to the charging.

What determines the conductance gap? The above discussion shows that the conductance gap is equal to $4(|E_f - \varepsilon_0| - \Delta)$, where Δ is equal to $\sim 4k_BT$ (plus $\Gamma_1 + \Gamma_2$ if broadening is included, see Section 12.3.3); and ε_0 is the HOMO or LUMO level, whichever is closest to the Fermi energy, as pointed out in Reference 34.

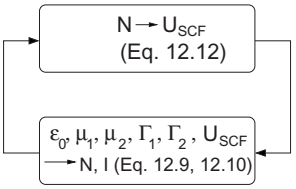

FIGURE 12.10 Illustration of the SCF problem.

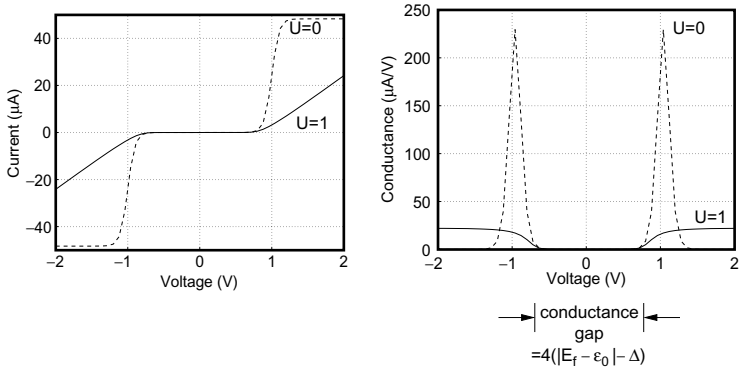

FIGURE 12.11 The current–voltage (I-V) characteristics (left) and conductance–voltage (G-V) (right) for our toy model with $E_f = -5.0$ eV, $\varepsilon_0 = -5.5$ eV and $\Gamma_1 = \Gamma_2 = 0.2$ eV. Solid lines, charging effects included ($U = 1.0$ eV). Dashed line, no charging ($U = 0$). MATLAB code in section 12.A.1.

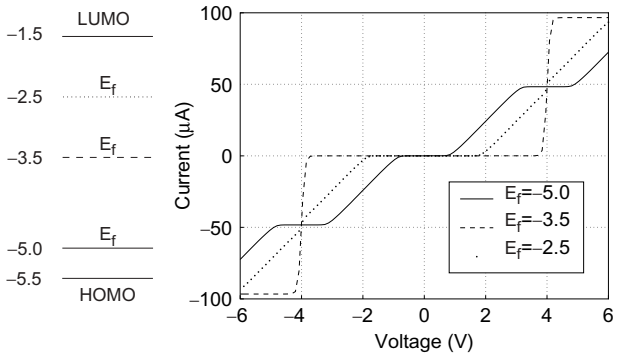

FIGURE 12.12 Right, the current–voltage (I-V) characteristics for the two level toy model for three different values of the Fermi energy (E_f). Left, the two energy levels (LUMO = –1.5 eV; HOMO = –5.5 eV) and the three different Fermi energies (–2.5, –3.5, –5.0) used in the calculations. (Other parameters used U = 1.0 eV; $\Gamma_1 = \Gamma_2$ = 0.2 eV) MATLAB code in Section 12.A.1.

This is unappreciated by many who associate the conductance gap with the HOMO–LUMO gap. However, we believe that what conductance measurements show is the gap between the Fermi energy and the nearest molecular level.* Figure 12.12 shows the I-V characteristics calculated using a two-level model (obtained by a straightforward extension of the one-level model) with the Fermi energy located differently within the HOMO–LUMO gap giving different conductance gaps corresponding to the different values of $|E_f - \varepsilon_0|$. Note that with the Fermi energy located halfway in between, the conductance gap is twice the HOMO–LUMO gap; and the I-V shows no evidence of charging effects because the depletion of the HOMO is neutralized by the charging of the LUMO. This perfect compensation is unlikely in practice, because the two levels will not couple identically to the contacts as assumed in the model.

A very interesting effect that can be observed is the asymmetry of the I-V characteristics of $\Gamma_1 \neq \Gamma_2$ as shown in Figure 12.13. This may explain several experimental results which show asymmetric I-V,[6,12] as discussed by Ghosh et al.[35] Assuming that the current is conducted through the HOMO level ($E_f > \varepsilon_0$), the current is less when a positive voltage is applied to the strongly coupled contact (Figure 12.13a). This is due to the effects of charging as has been discussed in more detail in Reference 35. Ghosh et al. also show that this result will reverse if the conduction is through the LUMO level. We can simulate this situation by setting ε_0 equal to –4.5 eV, 0.5 eV above the equilibrium Fermi energy E_f. The sense of

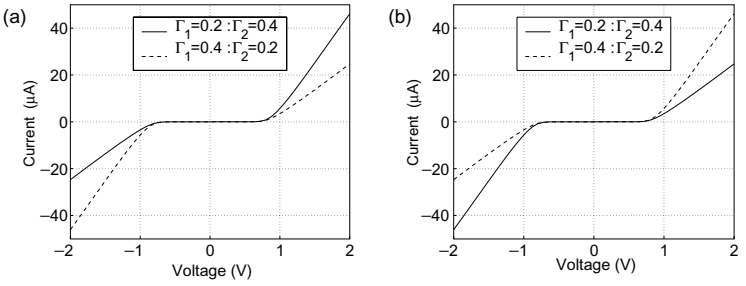

FIGURE 12.13 The current–voltage (I-V) characteristics for our toy model (E_f = –5.0 eV and U = 1.0 eV). (a) Conduction through LUMO ($E_f < \varepsilon_0$ = –4.5 eV). Solid lines, Γ_1 = 0.2 eV < Γ_2 = 0.4 eV. Dashed lines, Γ_1 = 0.4 eV > Γ_2 = 0.2 eV. MATLAB code in Section 12.A.1. Here positive voltage is defined as a voltage that lowers the chemical potential of contact 1.

*With very asymmetric contacts, the conductance gap could be equal to the HOMO–LUMO gap as commonly assumed in interpreting STM spectra. However, we believe that the picture presented here is more accurate unless the contact is so strongly coupled that there is a significant density of metal-induced gap states (MIGS).[28]

asymmetry is now reversed as shown in Figure 12.13b. The current is larger when a positive voltage is applied to the strongly coupled contact. Comparing with STM measurements seems to favor the first case, i.e., conduction through the HOMO.[35]

12.3.2 Unrestricted Model

In the previous examples (Figures 12.11 and 12.13) we have used values of $\Gamma_{1,2}$ that are smaller than the charging energy U. However, under these conditions one can expect CB effects, which are not captured by a *restricted solution*, which assumes that both spin orbitals see the same self-consistent field. However, an unrestricted solution, which allows the spin degeneracy to be lifted, will show these effects.* For example, if we replace Equation (12.13) with ($f_0 = f(\varepsilon_0, E_f)$):

$$\varepsilon_\uparrow = \varepsilon_0 + U(N_\downarrow - f_0) \tag{12.14}$$

$$\varepsilon_\downarrow = \varepsilon_0 + U(N_\uparrow - f_0) \tag{12.15}$$

where the up-spin level feels a potential due to the down-spin electrons and vice versa, then we obtain I-V curves as shown in Figure 12.14.

If the SCF iteration is started with a spin-degenerate solution, the same restricted solution as before is obtained. However, if the iteration is started with a spin-nondegenerate solution, a different I-V is obtained. The electrons only interact with the electron of the opposite spin. Therefore, the chemical potential of one contact can cross one energy level of the molecule because the charging of that level only affects the opposite spin level. Thus, the I-V contains two separate steps separated by U instead of a single step broadened by U.

For a molecule chemically bonded to a metallic surface, e.g., a PDT molecule bonded by a thiol group to a gold surface, the broadening Γ is expected to be of the same magnitude or larger than U. This washes out CB effects as shown in Figure 12.17. Therefore, the CB is not expected in this case. However, if the coupling to both contacts is weak, we should keep the possibility of CB and the importance of unrestricted solutions in mind.

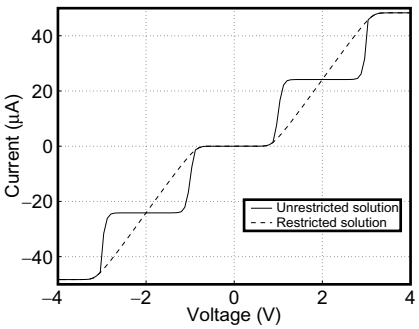

FIGURE 12.14 The current–voltage (I-V) characteristics for restricted (dashed line) and unrestricted solutions (solid line). $E_f = -5.0$ eV, $\Gamma_1 = \Gamma_2 = 0.2$ eV and $U = 1.0$ eV. MATLAB code in Sections 12.A.1 and 12.A.4.

* The unrestricted one-particle picture discussed here provides at least a reasonable qualitative picture of CB effects, though a complete description requires a more advanced many particle picture.[36] The one-particle picture leads to one of many possible states of the device depending on our initial guess, while a full many-particle picture would include all states.

12.3.3 Broadening

So far we have treated the level ε as discrete, ignoring the broadening $\Gamma = \Gamma_1 + \Gamma_2$ that accompanies the coupling to the contacts. To take this into account we need to replace the discrete level with a Lorentzian density of states $D(E)$:

$$D(E) = \frac{1}{2\pi}\frac{\Gamma}{(E-\varepsilon)^2 + (\Gamma/2)^2} \tag{12.16}$$

As we will see later, Γ is in general *energy-dependent* so that $D(E)$ can deviate significantly from a Lorentzian shape. We modify Equations (12.9) and (12.10) for N and I to include an integration over energy:

$$N = 2\int_{-\infty}^{\infty} dE D(E)\frac{\Gamma_1 f(E,\mu_1) + \Gamma_2 f(E,\mu_2)}{\Gamma_1 + \Gamma_2} \tag{12.17}$$

$$I = \frac{2e}{\hbar}\int_{-\infty}^{\infty} dE D(E)\frac{\Gamma_1\Gamma_2}{\Gamma_1 + \Gamma_2}(f(E,\mu_1) - f(E,\mu_2)) \tag{12.18}$$

The charging effect is included as before by letting the center ε, of the molecular density of states, float up or down according to Equations (12.12) and (12.13) for the restricted model or Equations (12.14) and (12.15) for the unrestricted model.

For the restricted model, the only effect of broadening is to smear out the I-V characteristics as evident from Figure 12.15. The same is true for the unrestricted model as long as the broadening is much smaller than the charging energy (Figure 12.16). But moderate amounts of broadening can destroy the Coulomb Blockade effects completely and make the I-V characteristics look identical to the restricted model (Figure 12.17). With this in mind, we will use the restricted model in the remainder of this chapter.

12.4 Nonequilibrium Green's Function (NEGF) Formalism

The one-level toy model described in the last section includes the three basic factors that influence molecular conduction, namely, $E_f - \varepsilon_0$, $\Gamma_{1,2}$, and U. However, real molecules typically have multiple levels that often broaden and overlap in energy. Note that the two-level model (Figure 12.12) in the last section treated the two levels as *independent,* and such models can be used only if the levels do not overlap. In general, we need a formalism that can do justice to multiple levels with arbitrary broadening and overlap. The nonequilibrium Green's function (NEGF) formalism described in this section does just that.

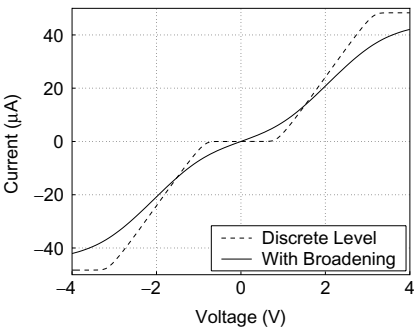

FIGURE 12.15 The current–voltage (I-V) characteristics: Solid line, include broadening of the level by the contacts. Dashed line, no broadening, same as solid line in Figure 12.11. MATLAB code in Sections 12.A.3 and 12.A.1 (E_f = –5.0 eV, ε_0 = –5.5, U = 1, and $\Gamma_1 = \Gamma_2$ = 0.2 eV).

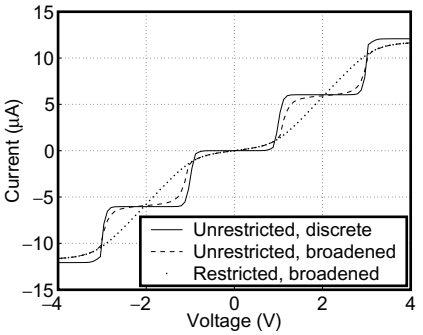

FIGURE 12.16 Current–voltage (I-V) characteristics showing the Coulomb blockade: discrete unrestricted model (solid line, MATLAB code in Section 12.A.4) and the broadened unrestricted mode (dashed line, 12.A.5). The dotted line shows the broadened restricted model without Coulomb blockade (12.A.3). For all curves the following parameters were used: $E_f = -5.0$, $\varepsilon_0 = -5.5$, $U = 1$, and $\Gamma_1 = \Gamma_2 = 0.05$ eV.

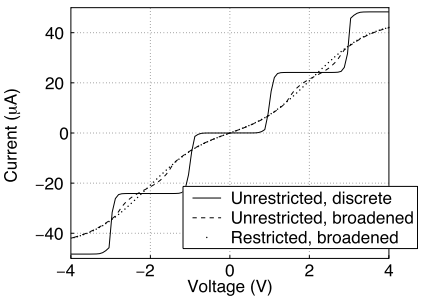

FIGURE 12.17 Current–voltage (I-V) characteristics showing the suppression of the Coulomb blockade by broadening: discrete unrestricted model (solid line) and the broadened unrestricted model (dashed line). The dotted line shows the broadened restricted model, $\Gamma_1 = \Gamma_2 = 0.2$ eV.

In the last section we obtained equations for the number of electrons N and the current I for a one-level model with broadening. It is useful to rewrite these equations in terms of the Green's function $G(E)$, defined as follows:

$$G(E) = \left(E - \varepsilon + i\frac{\Gamma_1 + \Gamma_2}{2}\right)^{-1} \tag{12.19}$$

The density of states $D(E)$ is proportional to the spectral function $A(E)$ defined as:

$$A(E) = -2\mathrm{Im}\{G(E)\} \tag{12.20}$$

$$D(E) = \frac{A(E)}{2\pi} \tag{12.21}$$

while the number of electrons N and the current I can be written as:

$$N = \frac{2}{2\pi}\int_{-\infty}^{\infty} dE(|G(E)|^2\Gamma_1 f(E, \mu_1) + |G(E)|^2\Gamma_2 f(E, \mu_2)) \tag{12.22}$$

$$I = \frac{2e}{h}\int_{-\infty}^{\infty} dE\Gamma_1\Gamma_2|G(E)|^2(f(E, \mu_1) - f(E, \mu_2)) \tag{12.23}$$

In the NEGF formalism the single energy level ε is replaced by a Hamiltonian matrix $[H]$, while the broadening $\Gamma_{1,2}$ is replaced by a complex energy-dependent self-energy matrix $[\Sigma_{1,2}(E)]$ so that the Green's function becomes a matrix given by

$$G(E) = (ES - H - \Sigma_1 - \Sigma_2)^{-1} \tag{12.24}$$

where S is the identity matrix of the same size as the other matrices, and the broadening matrices $\Gamma_{1,2}$ are defined as the imaginary (more correctly as the anti-Hermitian) parts of $\Sigma_{1,2}$:

$$\Gamma_{1,2} = i(\Sigma_{1,2} - \Sigma_{1,2}^{\dagger}) \tag{12.25}$$

The spectral function is the anti-Hermitian part of the Green's function:

$$A(E) = i(G(E) - G^{\dagger}(E)) \tag{12.26}$$

from which the density of states $D(E)$ can be calculated by taking the trace:

$$D(E) = \frac{\mathrm{Tr}(AS)}{2\pi} \tag{12.27}$$

The density matrix $[\rho]$ is given by, c.f., Equation (12.22):

$$\rho = \frac{1}{2\pi}\int_{-\infty}^{\infty}[f(E,\mu_1)G\Gamma_1 G^{\dagger} + f(E,\mu_2)G\Gamma_2 G^{\dagger}]\mathrm{d}E \tag{12.28}$$

from which the total number of electrons N can be calculated by taking a trace:

$$N = \mathrm{Tr}(\rho S) \tag{12.29}$$

The current is given by (c.f., Equation (12.23)):

$$I = \frac{2e}{h}\int_{-\infty}^{\infty}[\mathrm{Tr}(\Gamma_1 G\Gamma_2 G^{\dagger})(f(E,\mu_1) - f(E,\mu_2))]\mathrm{d}E \tag{12.30}$$

Equations (12.24) through (12.30) constitute the basic equations of the NEGF formalism, which have to be solved self-consistently with a suitable scheme to calculate the self-consistent potential matrix $[U_{SCF}]$ (c.f., Equation (12.13)):

$$H = H_0 + U_{SCF} \tag{12.31}$$

where H_0 is the bare Hamiltonian (like ε_0 in the toy model) and U_{SCF} is an appropriate functional of the density matrix ρ:

$$U_{SCF} = F(\rho) \tag{12.32}$$

This self-consistent procedure is essentially the same as in Figure 12.10 for the one-level toy model, except that scalar quantities have been replaced by matrices:

$$\varepsilon_0 \rightarrow [H_0] \tag{12.33}$$

$$\Gamma \rightarrow [\Gamma],\ [\Sigma] \tag{12.34}$$

$$N \rightarrow [\rho] \tag{12.35}$$

$$U_{SCF} \rightarrow [U_{SCF}] \tag{12.36}$$

The sizes of all these matrices is $(n \times n)$, n being the number of basis functions used to describe the *molecule*. Even the self-energy matrices $\Sigma_{1,2}$ are of this size although they represent the effect of infinitely large contacts. In the remainder of this section and the next section, we will describe the procedure used to evaluate the Hamiltonian matrix H, the self-energy matrices $\Sigma_{1,2}$, and the functional F used to evaluate the self-consistent potential U_{SCF} (see Equation (12.32)). But the point to note is that once we know how to evaluate these matrices, Equations (12.24) through (12.32) can be used straightforwardly to calculate the current.

Nonorthogonal basis: The matrices appearing above depend on the basis functions that we use. Many of the formulations in quantum chemistry use nonorthogonal basis functions; and the matrix Equations (12.24) through (12.32) are still valid as is, except that the elements of the matrix $[S]$ in Equation (12.24) represent the overlap of the basis function $\phi_m(\vec{r})$:

$$S_{mn} = \int d^3 r \phi_m^*(\vec{r}) \phi_n(\vec{r}) \tag{12.37}$$

For orthogonal bases, $S_{mn} = \delta_{mn}$ so that S is the identity matrix as stated earlier. The fact that the matrix Equations (12.24) through (12.32) are valid even in a nonorthogonal representation is not self-evident and is discussed in Reference 28.

Incoherent Scattering: One last comment about the general formalism: the formalism as described above neglects all incoherent scattering processes inside the molecule. In this form it is essentially equivalent to the Landauer formalism.[37] Indeed, our expression for the current (Equation (12.30)) is exactly the same as in the transmission formalism, with the transmission T given by $\mathrm{Tr}(\Gamma_1 G \Gamma_2 G^\dagger)$. But it should be noted that the real power of the NEGF formalism lies in its ability to provide a first-principles description of incoherent scattering processes — something we do not address in this chapter and leave for future work.

A practical consideration: Both Equations (12.28) and (12.30) require an integral over all energy. This is not a problem in Equation (12.30) because the integrand is nonzero only over a limited range, where $f(E, \mu_1)$ differs significantly from $f(E, \mu_2)$. But in Equation (12.28), the integrand is nonzero over a large energy range and often has sharp structures, making it numerically challenging to evaluate the integral. One way to address this problem is to write

$$\rho = \rho_{eq} + \Delta\rho \tag{12.38}$$

where ρ_{eq} is the equilibrium density matrix given by

$$\rho_{eq} = \frac{1}{2\pi} \int_{-\infty}^{\infty} f(E, \mu)[G\Gamma_1 G^\dagger + G\Gamma_2 G^\dagger] dE \tag{12.39}$$

and $\Delta\rho$ is the change in the density matrix under bias:

$$\Delta\rho = \frac{1}{2\pi} \int_{-\infty}^{\infty} G\Gamma_1 G^\dagger [f(E, \mu_1) - f(E, \mu)] + G\Gamma_2 G^\dagger [f(E, \mu_2) - f(E, \mu)] dE \tag{12.40}$$

The integrand in Equation (12.40) for $\Delta\rho$ is nonzero only over a limited range (like Equation (12.30) for I) and is evaluated relatively easily. The evaluation of ρ_{eq}(Equation (12.39)), however, still has the same problem; but this integral (unlike the original Equation (12.28)) can be tackled by taking advantage of the method of contour integration as described in References 38 and 39.

12.5 An Example: Quantum Point Contact (QPC)

Consider, for example, a gold wire stretched between two gold surfaces as shown in Figure 12.18. One of the seminal results of mesoscopic physics is that such a wire has a quantized conductance equal to $e^2/$

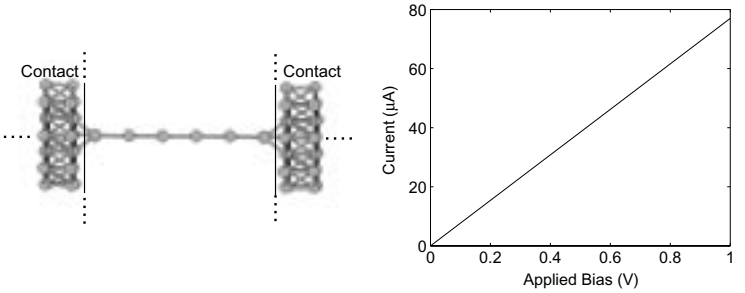

FIGURE 12.18 Left, wire consisting of six gold atoms forming a Quantum Point Contact (QPC). Right, quantized conductance ($I = (e^2/\pi\hbar)V$).

$\pi\hbar \sim 77.5\ \mu A/V \sim (12.9\ k\Omega)^{-1}$. This was first established using semiconductor structures[29,40,41] at 4 K, but recent experiments on gold contacts have demonstrated it at room temperature.[42] How can a wire have a resistance that is independent of its length? The answer is that this resistance is really associated with the interfaces between the narrow wire and the wide contacts. If there were scattering inside the wire, it would give rise to an additional resistance in series with this fundamental interface resistance. The fact that a short wire has a resistance of 12.9 kΩ is a nonobvious result that was not known before 1988. This is a problem for which we do not really need a quantum transport formalism; a semiclassical treatment would suffice. The results we obtain here are not new or surprising. What is new is that we treat the gold wire as an Au_6 molecule and obtain well-known results commonly obtained from a continuum treatment.

In order to apply the NEGF formalism from the last section to this problem, we need the Hamiltonian matrix $[H]$, the self-energy matrices $\Sigma_{1,2}$, and the self-consistent field $U_{SCF} = F([\rho])$. Let us look at these one by one.

Hamiltonian: We will use a simple semi-empirical Hamiltonian which uses one s-orbital centered at each gold atom as the basis functions, with the elements of the Hamiltonian matrix given by

$$\begin{aligned} H_{ij} &= \varepsilon_0 \qquad \text{if } i = j \\ &= -t \qquad \text{if } i, j \text{ are nearest neighbors} \end{aligned} \tag{12.41}$$

where $\varepsilon_0 = -10.92$ eV and $t = 2.653$ eV. The orbitals are assumed to be orthogonal, so that the overlap matrix S is the identity matrix.

Self Energy: Once we have a Hamiltonian for the entire molecule-contact system, the next step is to partition the device from the contacts and obtain the self-energy matrices $\Sigma_{1,2}$ describing the effects of the contacts on the device. The contact will be assumed to be essentially unperturbed relative to the surface of a bulk metal so that the full Green's function (G_T) can be written as (the energy E is assumed to have an infinitesimal imaginary part $i0^+$):

$$G_T = \begin{pmatrix} ES - H & ES_{dc} - H_{dc} \\ ES_{cd} - H_{cd} & ES_c - H_c \end{pmatrix}^{-1} = \begin{pmatrix} G & G_{dc} \\ G_{cd} & G_c \end{pmatrix} \tag{12.42}$$

where c denotes one of the contacts (the effect of the other contact can be obtained separately). We can use straightforward matrix algebra to show that:

$$G = (ES - H - \Sigma)^{-1} \tag{12.43}$$

$$\Sigma = (ES_{dc} - H_{dc})(ES_c - H_c)^{-1}(ES_{cd} - H_{cd}) \tag{12.44}$$

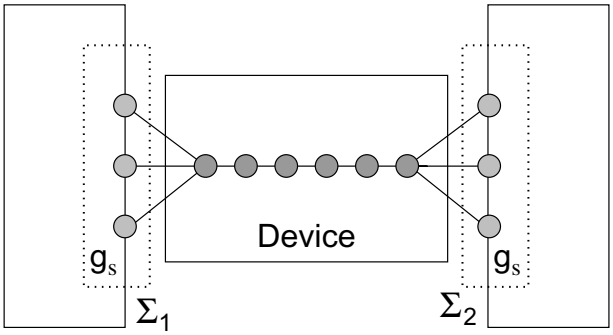

FIGURE 12.19 Device, surface Green's function (g_s) and self-energies (Σ).

The matrices S_{dc}, S_c, H_{dc}, and H_c are all infinitely large because the contact is infinite. But the element of S_{dc}, H_{dc} is nonzero only for a small number of contact atoms whose wave functions significantly overlap the device. Thus, we can write:

$$\Sigma = \tau g_s \tau^{\dagger} \tag{12.45}$$

where τ is the nonzero part of $ES_{dc}-H_{dc}$, having dimensions $(d \times s)$ where d is the size of the device matrix, and s is the number of surface atoms of the contact having a nonzero overlap with the device. g_s is a matrix of size $s \times s$ which is a subset of the full infinite-sized contact Green's function $(ES_c - H_c)^{-1}$. This surface Green's function can be computed exactly by making use of the periodicity of the semi-infinite contact, using techniques that are standard in surface physics.[31] For a one-dimensional lead, with a Hamiltonian given by Equation (12.41), the result is easily derived:[29]

$$g_s(E) = -\frac{e^{ika}}{t} \tag{12.46}$$

where ka is related to the energy through the dispersion relation:

$$E = \varepsilon_0 - 2t\cos(ka) \tag{12.47}$$

The results presented below were obtained using the more complicated surface Green's function for an FCC (111) gold surface as described in Reference 28. However, using the surface Green's function in Equation (12.46) gives almost identical results.

Electrostatic potential: Finally we need to identify the electrostatic potential across the device (Figure 12.20) by solving the Poisson equation:

$$-\nabla^2 U_{tot} = \frac{e^2 n}{\varepsilon_0} \tag{12.48}$$

with the boundary conditions given by the potential difference V_{app} between the metallic contacts (here ε_0 is the dielectric constant). To simplify the calculations we divide the solution into an applied and self-consistent potential ($U_{tot} = U_{app}+U_{SCF}$), where U_{app} solves the Laplace equation with the known potential difference between the metallic contacts:

$$\nabla^2 U_{app} = 0 \quad U_{app} = -eV_n \text{ on electrode n} \tag{12.49}$$

Thus, U_{tot} solves Equation (12.48) if U_{SCF} solves Equation (12.48) with zero potential at the boundary.

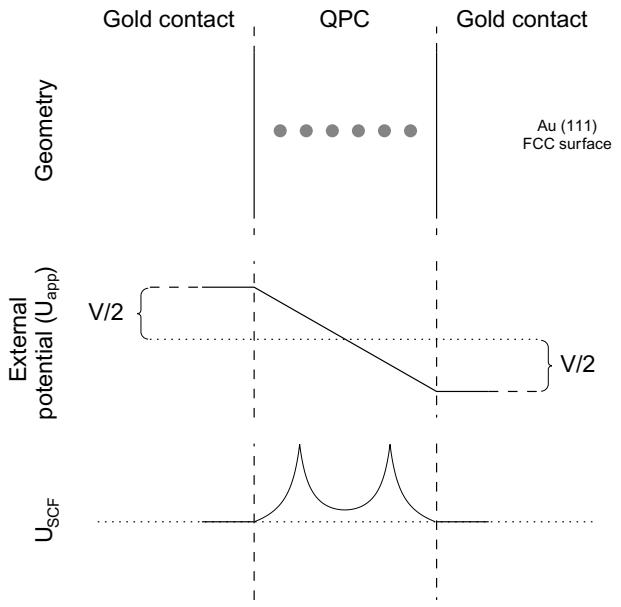

FIGURE 12.20 The electrostatic potentials divided into the applied (U_{app}) and the self-consistent field (U_{SCF}) potentials. The boundary conditions can clearly be seen in the figure; U_{SCF} is zero at the boundary and $U_{app} = \pm V_{app}/2$.

$$-\nabla^2 U_{SCF} = \frac{e^2 n}{\varepsilon_0} \quad U_{SCF} = 0 \text{ on all electrodes} \tag{12.50}$$

In the treatment of the electrostatic we assume the two contacts to be semi-infinite classical metals separated by a distance (W). This gives simple solutions to both U_{app} and U_{SCF}. The applied potential is given by (capacitor)

$$U_{app} = \frac{V}{W}x \tag{12.51}$$

where x is the position relative to the midpoint between the contacts. The self-consistent potential is easily calculated with the method of images where the potential is given by a sum over the point charges and all their images. However, to avoid the infinities associated with point charges, we adopt the Pariser–Parr–Pople (PPP) method[43,17] in the Hartree approximation. The PPP functional describing the electron–electron interactions is

$$H_{ij}^{e-e} = \delta_{ij} \sum_k (\rho_{kk} - \rho_{kk}^{eg}) \gamma_{ik} \tag{12.52}$$

where ρ is the charge density matrix, ρ^{eq} the equilibrium charge density (in this case ρ_{ii}^{eq} as we are modeling the s-electrons of gold), and the one-center two-electron integral γ_{ij}. The diagonal elements γ_{ii} are obtained from experimental data, and the off-diagonal elements (γ_{ij}) are parameterized to describe a potential that decreases as the inverse of the distance ($1/R_{ij}$):

$$\gamma_{ij} = \frac{e^2}{4\pi\varepsilon_0 R_{ij} + \dfrac{2e^2}{\gamma_{ii} + \gamma_{jj}}} \tag{12.53}$$

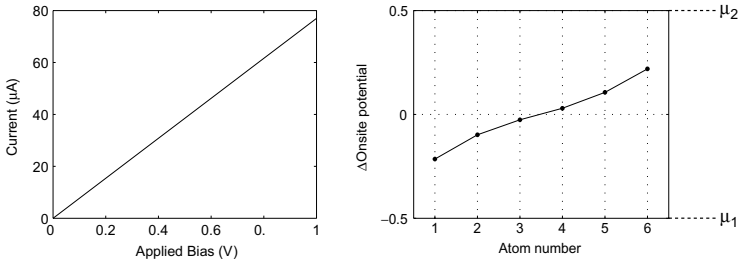

FIGURE 12.21 I-V (left) and potential drop for an applied voltage of 1 V (right) for a six-atom OPC connected to two contacts. The potential plotted is the difference in onsite potential from the equilibrium case.

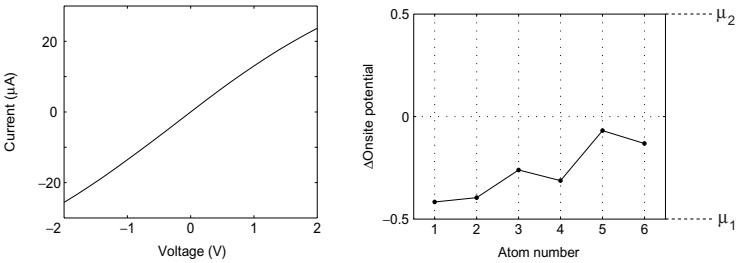

FIGURE 12.22 I-V and potential drop for an applied voltage of 1 V for the QPC asymmetrically connected the gold contacts. The coupling to the right contact used is –0.2*t*.

Calculations on the QPC: The results for the I-V and potential for a QPC are shown in Figure 12.21. The geometry used was a linear chain of six gold atoms connected to the FCC (111) surface of the contacts in the center of a surface triangle. The Fermi energy of the isolated contacts was calculated to be E_f = –8.67 eV, by requiring that there is one electron per unit cell.

As evident from the figure, the I-V characteristics are linear and the slope gives a conductance of 77.3 μA/V close to the quantized value of $e^2/\pi\hbar \sim 77.5$ μA/V as previously mentioned. What makes the QPC distinct from typical molecules is the strong coupling to the contacts, which broadens all levels into a continuous density of states; and any evidence of a conductance gap (Figure 12.2) is completely lost. Examining the potential drop over the QPC shows a linear drop over the center of the QPC with a slightly larger drop at the end atoms. This may seem surprising because transport is assumed to be *ballistic*, and one expects no voltage drop across the chain of gold atoms. This can be shown to arise because the chain is very narrow (one atom in cross-section) compared with the screening length.[19]

We can easily imagine an experimental situation where the device (QPC or molecule) is attached asymmetrically to the two contacts with one strong and one weak side. To model this situation we artificially decreased the interaction between the right contact and the QPC by a factor of 0.2. The results of this calculation are shown in Figure 12.22. A weaker coupling gives a smaller conductance, as compared with the previous figure. More interesting is that the potential drop over the QPC is asymmetric. Also in line with our classical intuition, the largest part of the voltage drop occurs at the weakly coupled contact with smaller drops over the QPC and at the strongly coupled contact. The consequences of asymmetric voltage drop over molecules has been discussed by Ghosh et al.[35]

12.6 Concluding Remarks

In this chapter we have presented an intuitive description of the current–voltage (I-V) characteristics of molecules using simple toy models to illustrate the basic physics (Sections 12.1–12.3). These toy models were also used to motivate the rigorous Nonequilibrium Green's Function (NEGF) theory (Section 12.4). A simple example was then used in Section 12.5 to illustrate the application of the NEGF formalism.

The same basic approach can be used in conjunction with a more elaborate Hückel Hamiltonian or even an *ab initio* Hamiltonian. But for these advanced treatments we refer the reader to References 27 and 28.

Some of these models are publicly available through the Purdue Simulation Hub (www.nanohub.purdue.edu) and can be run without any need for installation. In addition to the models discussed here, there is a Hückel model which is an improved version of the earlier model made available in 1999. Further improvements may be needed to take into account the role of inelastic scattering or polaronic effects, especially in longer molecules such as DNA chains.

Acknowledgments

Sections 12.2 and 12.3 are based on material from a forthcoming book by Supriyo Datta entitled *Quantum Phenomena: From Atoms to Transistors*. It is a pleasure to acknowledge helpful feedback from Mark Ratner, Phil Bagwell, and Mark Lundstrom. The authors are grateful to Prashant Damle and Avik Ghosh for helpful discussions regarding the *ab initio* models. This work was supported by the NSF under Grant No. 0085516–EEC.

12.7.A MATLAB® Codes

The MATLAB codes for the toy models can also be obtained at www.nanohub.purdue.edu.

12.7.A.1 Discrete One-Level Model

```
% Toy model, one level
% Inputs (all in eV)
E0 = -5.5;Ef = -5;gam1 = 0.2;gam2 = 0.2;U = 1;
%Constants (all MKS, except energy which is in eV)
hbar = 1.06e-34;q = 1.6e-19;IE = (2*q*q)/hbar;kT = .025;
% Bias (calculate 101 voltage points in [-4 4] range)
nV = 101;VV = linspace(-4,4,nV);dV = VV(2)-VV(1);
N0 = 2/(1+exp((E0-Ef)/kT));
for iV = 1:nV% Voltage loop
      UU = 0;dU = 1;
      V = VV(iV);mu1 = Ef-(V/2);mu2 = Ef+(V/2);
      while dU>1e-6%SCF
            E = E0+UU;
            f1 = 1/(1+exp((E-mu1)/kT));f2 = 1/(1+exp((E-mu2)/kT));
            NN = 2*((gam1*f1)+(gam2*f2))/(gam1+gam2);% Charge
            Uold = UU;UU = Uold+(.05*((U*(NN-N0))-Uold));
            dU = abs(UU-Uold);[V UU dU];
      end
      curr = IE*gam1*gam2*(f2-f1)/(gam1+gam2);
      II(iV) = curr;N(iV) = NN;[V NN];
end
G = diff(II)/dV;GG = [G(1) G];% Conductance
h = plot(VV,II*10^6,'k');% Plot I-V
```

12.7.A.2 Discrete Two-Level Model

```
% Toy model, two levels
% Inputs (all in eV)
Ef = -5;E0 = [-5.5 -1.5];gam1 = [.2 .2];gam2 = [.2 .2];U = 1*[1 1;1 1];
```

```
% Constants (all MKS, except energy which is in eV)
hbar = 1.06e-34;q = 1.6e-19;IE = (2*q*q)/hbar;kT = .025;
n0 = 2./(1+exp((E0-Ef)./kT));
nV = 101;VV = linspace(-6,6,nV);dV = VV(2)-VV(1);Usc = 0;
for iV = 1:nV
      dU = 1;
      V = VV(iV);mu1 = Ef+(V/2);mu2 = Ef-(V/2);
      while dU>1e-6
            E = E0+Usc;
            f1 = 1./(1+exp((E-mu1)./kT));f2 = 1./(1+exp((E-mu2)./kT));
            n = 2*(((gam1.*f1)+(gam2.*f2))./(gam1+gam2));
            curr = IE*gam1.*gam2.*(f1-f2)./(gam1+gam2);
            Uold = Usc;Usc = Uold+(.1*(((n-n0)*U')-Uold));
            dU = abs(Usc-Uold);[V Usc dU];
      end
      II(iV) = sum(curr);N(iV,:) = n;
end
G = diff(II)/dV;GG = [G(1) G];
h = plot(VV,II);% Plot I-V
```

12.7.A.3 Broadened One-Level Model

```
% Toy model, restricted solution with broadening
% Inputs (all in eV)
E0 = -5.5;Ef = -5;gam1 = 0.2;gam2 = 0.2;U = 1.0;
% Constants (all MKS, except energy which is in eV)
hbar = 1.06e-34;q = 1.6e-19;IE = (2*q*q)/hbar;kT = .025;
% Bias (calculate 101 voltage points in [-4 4] range)
nV = 101;VV = linspace(-4,4,nV);dV = VV(2)-VV(1);
N0 = 2/(1+exp((E0-Ef)/kT));
for iV = 1:nV% Voltage loop
      UU = 0;dU = 1;
      V = VV(iV);mu1 = Ef-(V/2);mu2 = Ef+(V/2);
      nE = 400;% Numerical integration over 200 points
      id = diag(eye(nE))';
      EE = linspace(-10,0,nE);dE = EE(2)-EE(1);
      f1 = 1./(1+exp((EE-id*mu1)/kT));
      f2 = 1./(1+exp((EE-id*mu2)/kT));
      while dU>1e-4% SCF
            E = E0+UU;
            g = 1./(EE-id*(E+i/2*(gam1+gam2)));
            NN = 2*sum(g.*conj(g).*(gam1*f1+gam2*f2))/(2*pi)*dE;
            Uold = UU;UU = Uold+(.2*((U*(NN-N0))-Uold));
            dU = abs(UU-Uold);[V UU dU];
      end
      curr = IE*gam1*gam2*sum((f2-f1).*g.*conj(g))/(2*pi)*dE;
      II(iV) = real(curr);N(iV) = NN;[V NN curr E mu1 mu2];
end
G = diff(II)/dV;GG = [G(1) G];% Conductance
h = plot(VV,II,'.'); Plot I-V
```

12.7.A.4 Unrestricted Discrete One-Level Model

```
% Toy model unrestricted solution
% Inputs (all in eV)
E0 = -5.5;Ef = -5;gam1 = 0.2;gam2 = 0.2;U = 1;
% Constants (all MKS, except energy which is in eV)
hbar = 1.06e-34;q = 1.6e-19;IE = (q*q)/hbar;kT = .025;
% Bias (calculate 101 voltage points in [-4 4] range)
nV = 101;VV = linspace(-4,4,nV);dV = VV(2)-VV(1);
N0 = 1/(1+exp((E0-Ef)/kT));
for iV = 1:nV% Voltage loop
      U1 = 0;U2 = 1e-5;dU1 = 1;dU2 = 1;
      V = VV(iV);mu1 = Ef-(V/2);mu2 = Ef+(V/2);
      while (dU1+dU2)>1e-6% SCF
            E1 = E0+U1;E2 = E0+U2;
            f11 = 1/(1+exp((E1-mu1)/kT));f21 = 1/(1+exp((E1-mu2)/kT));
            f12 = 1/(1+exp((E2-mu1)/kT));f22 = 1/(1+exp((E2-mu2)/kT));
            NN1 = ((gam1*f12)+(gam2*f22))/(gam1+gam2);
            NN2 = ((gam1*f11)+(gam2*f21))/(gam1+gam2);
            Uold1 = U1;Uold2 = U2;
            U1 = Uold1+(.05*((2*U*(NN1-N0))-Uold1));
            U2 = Uold2+(.05*((2*U*(NN2-N0))-Uold2));
            dU1 = abs(U1-Uold1);dU2 = abs(U2-Uold2);
      end
      curr1 = IE*gam1*gam2*(f21-f11)/(gam1+gam2);
      curr2 = IE*gam1*gam2*(f22-f12)/(gam1+gam2);
      (iV) = curr1;I2(iV) = curr2;
      N1(iV) = NN1;N2(iV) = NN2;[V NN1 NN2];
end
G = diff(I1+I2)/dV;GG = [G(1) G];% Conductance
h = plot(VV,I1+I2,'-'); Plot I-V
```

12.7.A.5 Unrestricted Broadened One-Level Model

```
% Toy model, unrestricted solution with broadening
% Inputs (all in eV)
E0 = -5.5;Ef = -5;gam1 = 0.2;gam2 = 0.2;U = 1;
% Constants (all MKS, except energy which is in eV)
hbar = 1.06e-34;q = 1.6e-19;IE = (q*q)/hbar;kT = .025;
% Bias (calculate 101 voltage points in [-4 4] range)
nV = 101;VV = linspace(-4,4,nV);dV = VV(2)-VV(1);
N0 = 1/(1+exp((E0-Ef)/kT));
nE = 200;% Numerical integration over 200 points
id = diag(eye(nE))';
EE = linspace(-9,-1,nE);dE = EE(2)-EE(1);
for iV = 1:nV% Voltage loop
      U1 = 0;U2 = 1;dU1 = 1;dU2 = 1;
      V = VV(iV);mu1 = Ef-(V/2);mu2 = Ef+(V/2);
      f1 = 1./(1+exp((EE-id*mu1)/kT));
      f2 = 1./(1+exp((EE-id*mu2)/kT));
      while (dU1+dU2)>1e-3% SCF
            E1 = E0+U1;E2 = E0+U2;
```

```
            g1 = 1./(EE-id*(E1+i/2*(gam1+gam2)));
            g2 = 1./(EE-id*(E2+i/2*(gam1+gam2)));
            NN1 = sum(g1.*conj(g1).*(gam1*f1+gam2*f2))/(2*pi)*dE;
            NN2 = sum(g2.*conj(g2).*(gam1*f1+gam2*f2))/(2*pi)*dE;
            Uold1 = U1;Uold2 = U2;
            U1 = Uold1+(.2*((2*U*(NN2-N0))-Uold1));
            U2 = Uold2+(.2*((2*U*(NN1-N0))-Uold2));
            dU1 = abs(U1-2*U*(NN2-N0));dU2 = abs(U2-2*U*(NN1-N0));
      end
      curr = IE*gam1*gam2*sum((f2-f1).*(g1.*conj(g1)+...
      g2.*conj(g2)))/(2*pi)*dE;
      II(iV) = real(curr);N(iV) = NN1+NN2;
      [V NN1 NN2 curr*1e6 E1 E2 mu1 mu2];
end
G = diff(II)/dV;GG = [G(1) G];% Conductance
h = plot(VV,II,' - ');% Plot I-V
```

References

1. P. Avouris, P.G. Collins, and M.S. Arnold. Engineering carbon nanotubes and nanotube circuits using electrical breakdown. *Science*, 2001.
2. A. Bachtold, P. Hadley, T. Nakanishi, and C. Dekker. Logic circuits with carbon nanotube transistors. *Science*, 294:1317, 2001.
3. H. Schön, H. Meng, and Z. Bao. Self-assembled monolayer organic field-effect transistors. *Nature*, 413:713, 2001.
4. R.P. Andres, T. Bein, M. Dorogi, S. Feng, J.I. Henderson, C.P. Kubiak, W. Mahoney, R.G. Osifchin, and R. Reifenberger. "Coulomb staircase" at room temperature in a self-assembled molecular nanostructure. *Science*, 272:1323, 1996.
5. M.A. Reed, C. Zhou, C.J. Muller, T.P. Burgin, and J.M. Tour. Conductance of a molecular junction. *Science*, 278:252, 1997.
6. C. Kergueris, J.-P. Bourgoin, D. Esteve, C. Urbina, M. Magoga, and C. Joachim. Electron transport through a metal–molecule–metal junction. *Phys. Rev. B*, 59(19):12505, 1999.
7. C. Kergueris, J.P. Bourgoin, and S. Palacin. Experimental investigations of the electrical transport properties of dodecanethiol and α, ω bisthiolterthiophene molecules embedded in metal–molecule–metal junctions. *Nanotechnology*, 10:8, 1999.
8. J. Reichert, R. Ochs, H.B. Weber, M. Mayor, and H.V. Löhneysen. Driving current through single organic molecules. *cond-mat/0106219*, June 2001.
9. S. Hong, R. Reifenberger, W. Tian, S. Datta, J. Henderson, and C.P. Kubiak. Molecular conductance spectroscopy of conjugated, phenyl-based molecules on au(111): the effect of end groups on molecular conduction. *Superlattices Microstruct.,* 28:289, 2000.
10. J.J.W.M. Rosink, M.A. Blauw, L.J. Geerligs, E. van der Drift, and S. Radelaar. Tunneling spectroscopy study and modeling of electron transport in small conjugated azomethine molecules. *Phys. Rev. B*, 62(15):10459, 2000.
11. C. Joachim and J.K. Gimzewski. An electromechanical amplifier using a single molecule. *Chem. Phys. Lett.*, 265:353, 1997.
12. W. Tian, S. Datta, S. Hong, R. Reifenberger, J.I. Henderson, and P. Kubiak. Conductance spectra of molecular wires. *J. Chem. Phys.*, 109(7):2874, 1998.
13. J. Chen, W. Wang, M.A. Reed, A.M. Rawlett, D.W. Price, and J.M. Tour. Room-temperature negative differential resistance in nanoscale molecular junctions. *Appl. Phys. Lett.*, 77(8):1224, 2000.
14. D. Porath, A. Bezryadin, S. de Vries, and C. Dekker. Direct measurement of electrical transport through DNA molecules. *Nature*, 403:635, 2000.

15. M. Magoga and C. Joachim. Conductance of molecular wires connected or bonded in parallel. *Phys. Rev. B*, 59(24):16011, 1999.
16. L.E. Hall, J.R. Reimers, N.S. Hush, and K. Silverbrook. Formalism, analytical model, and *a priori* Green's function-based calculations of the current–voltage characteristics of molecular wires. *J. Chem. Phys.*, 112:1510, 2000.
17. M. Paulsson and S. Stafström. Self-consistent field study of conduction through conjugated molecules. *Phys. Rev. B*, 64:035416, 2001.
18. E.G. Emberly and G. Kirczenow. Multiterminal molecular wire systems: a self-consistent theory and computer simulations of charging and transport. *Phys. Rev. B*, 62(15):10451, 2000.
19. P.S. Damle, A.W. Ghosh, and S. Datta. Unified description of molecular conduction: from molecules to metallic wires. *Phys. Rev. B*, 64:201403(r), 2001.
20. J. Taylor, H. Gou, and J. Wang. *Ab initio* modeling of quantum transport properties of molecular electronic devices. *Phys. Rev. B*, 63:245407, 2001.
21. M. Di Ventra, S.T. Pantelides, and N.D. Lang. First-principles calculation of transport properties of a molecular device. *Phys. Rev. Lett.*, 84:979, 2000.
22. P. Damle, A.W. Ghosh, and S. Datta. First-principles analysis of molecular conduction using quantum chemistry software. *Chem. Phys.*, 281, 171, 2001.
23. Y.Q. Xue, S. Datta, and M.A. Ratner. Charge transfer and "band lineup" in molecular electronic devices: a chemical and numerical interpretation. *J. Chem. Phys.*, 115:4292, 2001.
24. J.J. Palacios, A.J. Pérez–Jiménez, E. Louis, and J.A. Vergés. Fullerene-based molecular nanobridges: a first-principles study. *Phys. Rev. B*, 64(11):115411, 2001.
25. J.M. Seminario, A.G. Zacarias, and J.M. Tour. Molecular current–voltage characteristics. *J. Phys. Chem. A*, 1999.
26. S. Datta. Nanoscale device modeling: the Green's function method. *Superlattices Microstruct.*, 28:253, 2000.
27. P.S. Damle, A.W. Ghosh, and S. Datta. Molecular nanoelectronics, in M. Reed (Ed.), *Theory of Nanoscale Device Modeling.* (To be published in 2002; for a preprint, e-mail: datta@purdue.edu.)
28. F. Zahid, M. Paulsson, and S. Datta. Advanced semiconductors and organic nano-techniques, in H. Markoc (Ed.), *Electrical Conduction through Molecules*. Academic Press. (To be published in 2002; for a preprint, e-mail: datta@purdue.edu.)
29. S. Datta. *Electronic Transport in Mesoscopic Systems*. Cambridge University Press, Cambridge, UK, 1997.
30. S.G. Lias et al. Gas-phase ion and neutral thermochemistry, *J. Phys. Chem*. Reference Data. American Chemical Society and Americal Institute of Physics, 1988.
31. C. Desjoqueres and D. Spanjaard. *Concepts in Surface Physics*. 2nd ed. Springer-Verlag, Berlin, 1996.
32. R.G. Parr and W. Yang. *Density Functional Theory of Atoms and Molecules*, Oxford University Press, 1989, p.99
33. de Picciotto, H.L. Stormer, L.N. Pfeiffer, K.W. Baldwin, and K.W. West. Four-terminal resistance of a ballistic quantum wire. *Nature*, 411:51, 2001.
34. S. Datta, W. Tian, S. Hong, R. Reifenberger, J.I. Henderson, and C.P. Kubiak. Current–voltage characteristics of self-assembled monolayers by scanning tunneling microscopy. *Phys. Rev. Lett.*, 79:2530, 1997.
35. A.W. Ghosh, F. Zahid, P.S. Damle, and S. Datta, Insights from I-V asymmetry in molecular conductors. Preprint. *cond-mat/0202519.*
36. Special issue on single-charge tunneling, *Z. Phys.B.,* 85, 1991.
37. P.F. Bagwell and T.P. Orlando. Landauer's conductance formula and its generalization to finite voltages. *Phys. Rev. B*, 40(3):1456, 1989.
38. M. Brandbyge, J. Taylor, K. Stokbro, J.-L. Mozos, and P. Ordejon. Density functional method for nonequilibrium electron transport. *Phys. Rev. B*, 65(16):165401, 2002.
39. R. Zeller, J. Deutz, and P. Dederichs. *Solid State Commun.*, 44:993, 1982.
40. Y. Imry. *Introduction to Mesoscopic Physics*. Oxford University Press, Oxford, 1997.

41. D.K. Ferry and S.M. Goodnick. *Transport in Nanostructures*. Cambridge University Press, London, 1997.
42. K. Hansen, E. Laegsgaard, I. Stensgaard, and F. Besenbacher. Quantized conductance in relays. *Phys. Rev. B*, 56:1022, 1997.
43. J.N. Murrell and A.J. Harget. *Semi-Empirical SCF MO Theory of Molecules*. John Wiley & Sons, London, 1972.